Shock Waves (1995) 4:247–252

Shock Waves

Experiments on the Richtmyer-Meshkov instability of an air/SF_6 interface

M. Vetter*, B. Sturtevant

Graduate Aeronautical Laboratories, California Institute of Technology, Pasadena, CA 91125, USA

Received August 26, 1994 / Accepted November 14, 1994

Abstract. Results of flow visualization experiments of an impulsively accelerated plane interface between air and SF_6 are reported. The shock tube used for the experiments has a larger test section than in previous experiments. The larger extent of uniform test flow relative to nonuniform boundary-layer flow permits unambiguous interpretation of flow-visualization photographs, and the influence of shock-wave/boundary-layer interactions is no longer dominant. The strong wall vortex observed in previous studies is not observed in these experiments. It is found that the thin membrane, which forms the initially plane interface, has a significant influence on the initial growth rate of the interface thickness. However, the measured growth rates after the first reflected shock are independent of membrane configuration and are in good agreement with analytical predictions.

Key words: Richtmyer-Meshkov instability, Flow visualization, Experiment, Shock tube, Turbulent mixing

1 Introduction

The Richtmyer-Meshkov instability occurs when a shock wave impinges upon an interface between two fluids of different densities (Richtmyer 1960; Meshkov 1969). The refraction of the shock wave from spatial perturbations on the interface causes distortion of both the interface and the shock wave. Most of the experiments so far reported in this field have concentrated on the instability of an initially sinusoidal interface with perturbations of wavelength λ and amplitude η_0. Richtmyer (1960) showed, that in this case the perturbation amplitude η grows linearly with time,

$$\frac{d\eta(t)}{dt} = \frac{2\pi}{\lambda}[u]A'\eta_0' \,, \tag{1}$$

where $[u]$ is the change of interface velocity induced by the shock wave, A' is the post-shock Atwood ratio and η_0' is the post-shock amplitude of the perturbation. The relation is only valid as long as $\eta(t) << \lambda$ or $t << \lambda^2/(\eta_0[u])$. However, small-scale perturbations, which are the subject of this paper, grow rapidly into the non-linear regime. Perturbations of, for example, $\eta_o/\lambda = 0.1$ and $\lambda = 1$ cm, on an interface which is accelerated impulsively from rest to a velocity of 150 m/s (all values typical for the experiments described here), will grow out of the linear regime within 0.7 ms. This finally leads to a turbulent mixing zone (TMZ) between the two fluids. Mikaelian (1989) adapted results of constant-acceleration experiments of Read (1984) to impulsive acceleration and obtained an analytical expression for the non-linearly saturated shock-induced thickening of an initially flat interface,

$$\delta = 0.28[u]A't \,, \tag{2}$$

where δ is the interface thickness. It has recently been suggested (Brouillette and Sturtevant 1989, 1993) that, due to the modest-size shock tubes used for the relatively few experiments on this problem to date (Andronov et al. 1976, Andronov et al. 1982, Brouillette and Sturtevant 1989, 1993), shock-wave/boundary-layer effects have had a large influence on the measured growth rates and on the interpretation of flow visualization pictures. The goal of this work is to reduce this influence by using a larger test section. Table 1 shows a comparison between previously used facilities and the present one. Also listed are the fluids used and incident shock Mach numbers M_s in these facilities. In the work reported here single high-resolution spark-schlieren photographs of the flow were obtained to exhibit the turbulent structure. High-speed schlieren motion pictures (35000–40000 frames per second) with a lower resolution were also used in order to measure the time evolution of the TMZ during each experiment. A better understanding of the influence and behavior of the membrane was obtained by using different knife edge orientations for the schlieren system and by fragmenting the membrane immediately after shock passage with a wire mesh placed downstream of the membrane.

2 Experimental

The experiments were performed in the GALCIT 17-inch diameter horizontal shock tube (Liepmann et al. 1962, Budzin-

* On leave from Stosswellenlabor (Shock Wave Laboratory), RWTH Aachen, Templergraben 55, D-52056 Aachen, Germany

Table 1. Comparison of facilities used in the field of Richtmyer-Meshkov instabilities

Reference	Test section dimensions [cm x cm]	Fluids	Shock Mach numbers M_s
Meshkov (1969)	12 x 4	air/CO_2 ; air/R22 ; air/He	1.52
Brouillette & Sturtevant (1993)	11.4 x 11.4	air/He ; air/CO_2 ; air/R22 ; air/SF_6	1.12–1.66
Andronov et al. (1976)	12 x 4	air/He	1.30
Benjamin (1992)	7.5 x 7.5	air/SF_6 ; air/He	1.24
Landeg et al. (1993)	20 x 5	R12/air	1.26
Youngs (1989)	15 x 15	pentane/SF_6; alcohol/air[a]	- [b]
present work	26.7 x 26.7	air/SF_6	1.18–1.98

[a] liquid/gas, [b] constant acceleration experiments

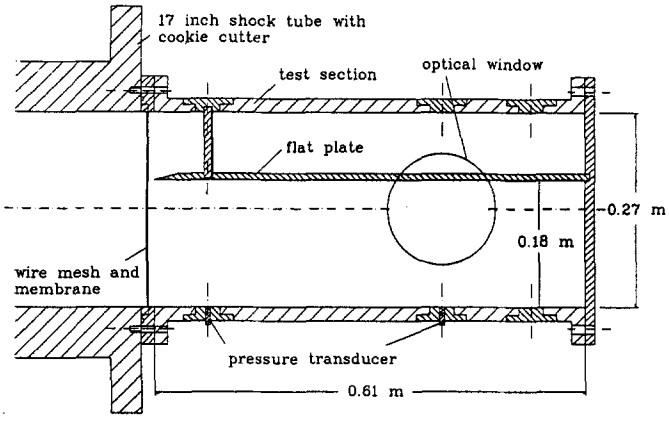

Fig. 1. Geometry of the short test section with the mounted flat plate

sky 1992). A 27 cm square test section is flanged to the end of this tube, and the transition from circular to square cross section is made with a cookie-cutter extending 1.5 m upstream into the shock tube. Depending on the test conditions either a long (1.22 m) or a short (0.61 m) test section is used (Fig. 1). A thin (0.5 μm) nitro-cellulose membrane, which forms the initial interface, is placed between the shock tube and the test section. Since the test section and especially the optical windows were not designed for large overpressures, Mach numbers above 1.1 can only be achieved by reducing the initial pressure p_1 below atmospheric. For $M_s = 2$ p_1 must be as low as 8 kPa. For this reason both the tube and the test section must first be evacuated before they can be filled with the desired gases. This procedure turned out to be the most difficult part of these experiments. In most of the experiments a wire mesh was installed to support the membrane on the upstream side during the filling procedure. In one configuration the mesh had a spacing of 10 mm both in the horizontal and vertical direction (wire diameter 0.23 mm). Prior to each run, the membrane was usually pushed slightly into the wire mesh, with an estimated amplitude of about 1 mm. To examine the effect of the mesh and the membrane, a few experiments were performed with the wire mesh placed on the downstream side of the membrane to fragment it. This made the pumping and filling process much more difficult. In addition, two partial meshes were constructed, one with vertical wires, and the other with horizontal wires, spaced on 1 cm centers. In order to complete the study of membrane effects, some runs were made with the membrane sandwiched between the two partial meshes. The optical windows for the schlieren visualization system are centered 42 cm downstream of the membrane and are 15 cm in diameter, so the shock tube wall is not directly visible in the pictures. Therefore, some experiments were performed with a sharp-edged flat plate mounted across the window, extending from the endwall up to a distance of 10 mm downstream of the membrane (Fig. 1).

For high-resolution imaging, a single spark-schlieren photograph was taken in each run. The spark source generates a flash of visible light of approximately 0.5 μs duration. With this approach the measurement of the evolution of the TMZ depends on the repeatability of flow conditions from run to run (Liepmann et al. 1962), and many runs are required. To overcome this shortcoming, lower resolution schlieren images were obtained with a Cordin Model 374A high-speed camera, permitting the observation of the entire time evolution in one experiment. Since flow features are not as clear in the high-speed motion pictures, it is important that the spark schlieren images were available to facilitate the interpretation. The thickness δ of the interface, defined to be the mean horizontal overall extent of the interface, was measured on both spark-schlieren and high-speed movie photographs. No corrections were made for possible wall effects. The rate of increase of the interface thickness ('growth rate') is obtained by a straight-line least-squares fit to the thickness data. For all experiments reported here the standard deviation of the least squares fits are of the order of 1 m/s after the incident shock and 2.5 m/s after the reflected shock.

Figure 2 shows the wave diagram, based on experimental data, of an air/SF_6 interface (density ratio 0.2) accelerated by a $M_s = 1.50$ shock wave at an initial pressure $p_1 = 23$ kPa. A $M_T = 1.78$ shock is transmitted into SF_6 and the interface is accelerated to about $u_0 = 150$ m/s. The circles indicate the times when spark schlieren pictures were taken. The relatively weak reflected expansion fan from the high pressure section of the shock tube that follows 0.5 ms after the incident shock, is not shown. The interaction of the shock reflected from the endwall with the interface occurs a short distance downstream of the optical window (represented by the two vertical lines). The interface then reverses its motion and is finally decelerated nearly to rest by the re-reflected expansion wave.

3 Flow visualization

Figure 3 shows some spark schlieren pictures of the interface after both the incident and reflected shocks. The quoted

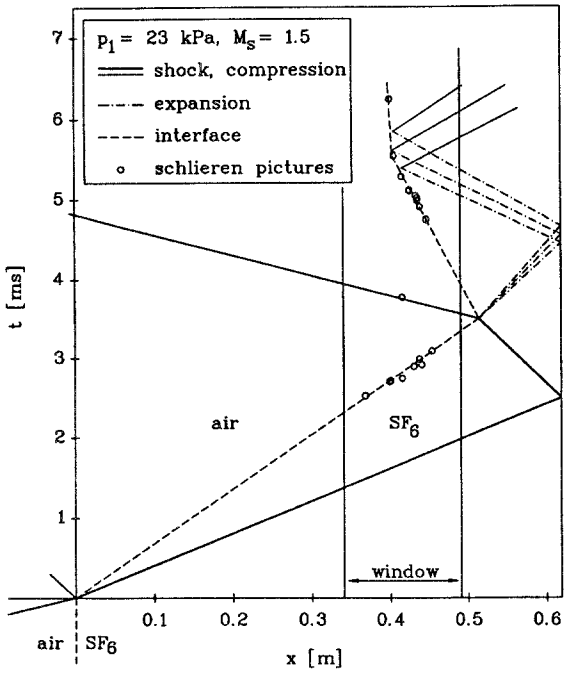

Fig. 2. Wave diagram for the interaction of a M_s = 1.50 shock wave with a plane discontinuous interface between air and SF_6

times are measured as in Fig. 2. In Fig. 3a, at t = 2.75 ms, the interface is travelling from left to right (the incident shock has already passed the window) and the membrane (thick black band) appears continuous, with some visible smooth undulations of wavelength approximately equal to that of the mesh. The mixing zone extends from a small distance behind the membrane to a larger distance ahead, suggesting that the membrane accelerated more slowly than the interface, and that the membrane is at least partially ruptured. The streaky structure visible behind the interface is caused by turbulent mixing of air and SF_6 in the boundary layers on the viewing windows. In order to demonstrate the difference between wall and core-flow features, Fig. 4a shows the interface at nearly the same time, but with the schlieren knife edge set vertical instead of horizontal, and with the flat plate mounted in the test section. Comparison of Figs 3a and 4a shows that the rear (left) dark band is indeed the membrane, since its appearance is independent of the knife edge orientation. However, now there is a forward dark band which is clearly a schlieren effect caused by large horizontal gradients at the front of the TMZ. What is observed in Fig. 4a is simply that the TMZ and membrane are bent forward near the plate, rather than being dragged back by viscous deceleration as might have been expected. This may be caused by a small misalignment of the flat plate, and is therefore likely not representative of the situation at the other side walls. Behind the membrane on the flat plate a boundary-layer with large density gradients can be observed. As described below, the measured growth rate after passage of the incident shock is much smaller than predicted by theory. To clarify the influence of the membrane, the wire mesh was placed on the downstream side of the membrane to fragment it and enhance mixing. The result is shown in Fig. 4b, an image of an interface after interaction with the incident shock at t = 2.83 ms. The mixing region is now much wider (cf. Fig. 3a) and the flow structure is not as uniform as before; the rear part is more curved than the front. Behind the TMZ are visible residual wakes of SF_6 from the wire mesh. The interface is five times thicker than with the wire mesh on the upstream side. However, this still represents a growth rate only about 2/3 of that predicted by Eq. (2). Figures 3b and 3c show the interface after interaction with the reflected shock. The interface thickness now grows rapidly, and fragments of the membrane are distributed over a much larger region. Again, it is clear that a vertical knife edge, (Fig. 3b), gives a better contrast regarding the TMZ, whereas a horizontal one, (Fig. 3c), provides a better view of the membrane itself. The fragments of the membrane roll up into thin strips, which are twisted around each other and tend to have arcuate form. As shown by Fig. 4c, a 'loop' or wall vortex, which was observed by other authors (Brouillete and Sturtevant 1993; Andronov et al. 1976) is not seen here. The membrane region very close to the plate seems to have been disturbed by the reflected shock, perhaps because of the forward bend seen in Fig. 4a, but the bulges at the front and rear further away from the plate are typical of our observations (cf. Fig. 3b and 3c) and in some cases are repeatable with or without the wall, do not extend to the wall and obviously do not wrap all around the test section.

4 Growth rates

Figure 5 shows the time evolution of the average thickness δ of the interface measured from single-spark photographs for M_s =1.50, 1.45 and 1.18 (growth rates were measured mainly from pictures made with a horizontal knife edge orientation). The experiments at the lowest shock Mach number were performed with the long test section, so the reflected interface was very thick when it came back into the field of view. For this reason there is only one datum available for its reflected shock thickness. The straight solid lines indicate results of least squares fits through the data before and after the arrival of the reflected shock (RS). The growth rates calculated assuming that the initial thickness is zero are given in Table 2. The index "0" corresponds to the conditions after the incident shock and the index "1" to those after the reflected shock. The effective initial thickness, due to the starting process, may in fact be finite. Thus the values given for the growth rates after the initial shock are upper bounds. They are approximately an order of magnitude smaller than predicted by Eq. (2). The growth rates after the reflected shock are in good agreement with Eq. (2) (indicated by the dash-dotted lines, using the Atwood ratios after the reflected shock), even for the low Mach number with only one datum available.

The evolution of the average thickness measured from the high-speed motion pictures for four different incident shock Mach numbers between 1.24 and 1.98 is shown in Fig. 6. The length L of the test section was adjusted in some experiments to insure that the interaction of the reflected shock wave with the interface would be in the field of view. The high-speed motion picture data agree with and extend the spark schlieren results. Very small and sometimes no growth is observed before the reflected shock interacts with the interface. Assuming that the growth is linear in time and

Table 2. Test conditions and comparison between measured and predicted growth rates of the interface thickness

	I[a]	II[b]	III[b]	IV[a]	V[a]	VI[b]	VII[b]	
M_s	1.18	1.24	1.43	1.45	1.50	1.50	1.98	-
p_1	55	40	31	29	23	23	8	kPa
L	123	110	62	62	62	62	49	cm
M_T	1.27	1.37	1.67	1.70	1.78	1.78	2.56	-
u_0	56	72	126	126	150	150	287	m/s
$(d\delta/dt)_{0,exp.}$	0.94	2.1	3.0	3.1	4.0	4.2	7.5	m/s
$(d\delta/dt)_{0,Eq.\ (2)}$	10.7	14.2	25.5	25.6	30.7	30.7	61.3	m/s
$(d\delta/dt)_{1,exp.}$	19.2	17.0	31.5	35.5	32.6	37.2	74.4	m/s
$(d\delta/dt)_{1,Eq.\ (2)}$	20.1	22.2	35.9	37.3	39.8	39.8	75.5	m/s

[a] results from single spark-schlieren photographs [b] results from high-speed motion pictures

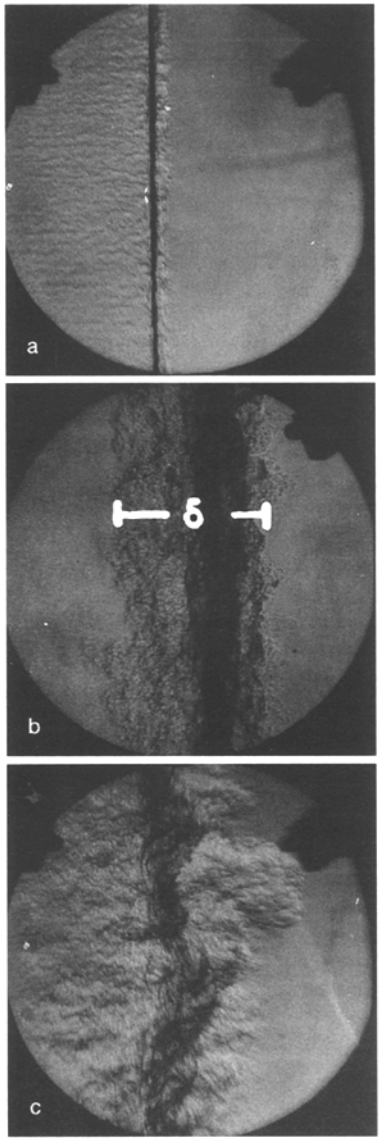

Fig. 3. Spark schlieren photographs of the Richtmyer-Meshkov instability of a plane discontinuous interface between air and SF_6. M_s = 1.50, short test section, window size 15 cm, mesh spacing 1 cm. (a) t = 2.75 ms, (b) t = 5.11 ms, (c) t = 5.55 ms

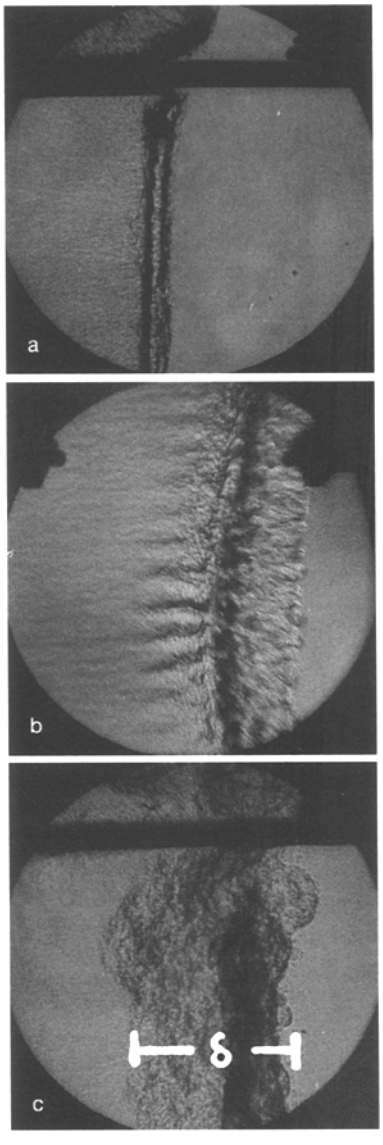

Fig. 4. Spark schlieren photographs of the Richtmyer-Meshkov instability of a plane discontinuous interface between air and SF_6. M_s = 1.50, short test section, window size 15 cm, mesh spacing 1 cm. (a) t = 2.71 ms, flat plate, (b) t = 2.83 ms, wire mesh on downstream side of membrane, (c) t = 5.02 ms, flat plate

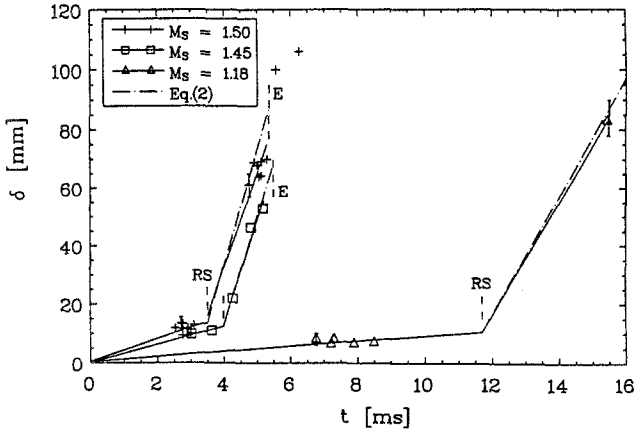

Fig. 5. Time evolution of the thickness of the TMZ for the plane discontinuous interface between air and SF_6. Results from spark schlieren pictures (RS: reflected shock; E: expansion)

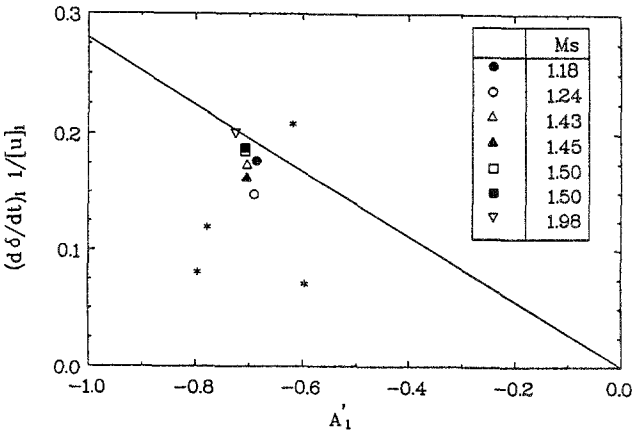

Fig. 7. Correlation of reflected shock growth rates for a discontinuous interface between air and SF_6; filled symbols: results from single schlieren pictures; open symbols: results from high speed motion pictures; —: Mikaelian formula (Eq. (2)); *: exp. results from Brouillette and Sturtevant

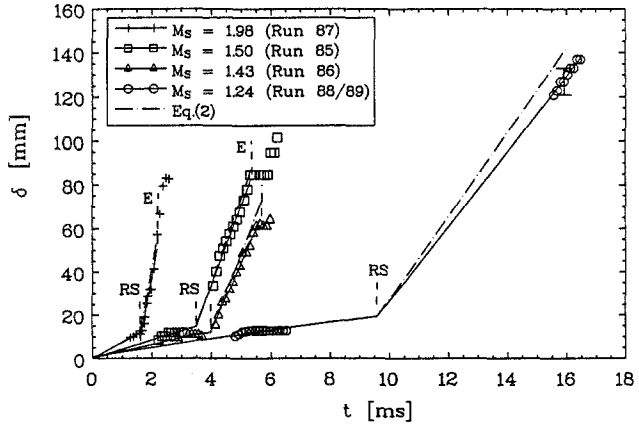

Fig. 6. Time evolution of the thickness of the TMZ for the plane discontinuous interface between air and SF_6. Results from high-speed motion pictures (RS: reflected shock; E: expansion)

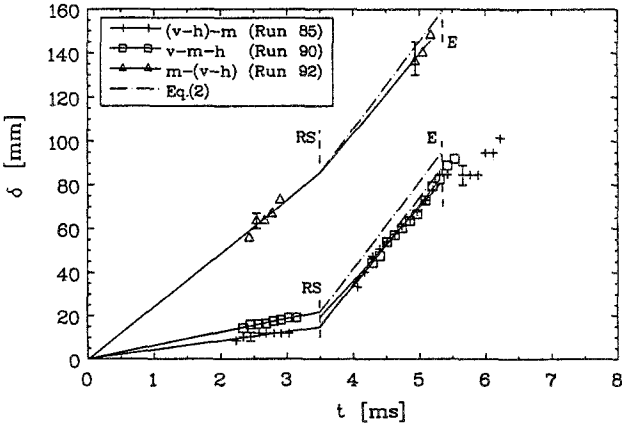

Fig. 8. Time evolution of the thickness of the TMZ for the plane discontinuous interface between air and SF_6; results from high-speed motion pictures; M_s = 1.50; the legend shows the wire mesh-membrane arrangement between air and SF_6: v-vertical wire mesh, h-horizontal wire mesh, m-membrane (RS: reflected shock; E: expansion)

performing a least squares fit again yields growth rates an order of magnitude smaller than Eq. (2). The growth of the interface between reflected shock and the arrival of the re-reflected expansion wave appears to be linear, and straight-line least squares fits yield growth rates in good agreement with Eq. (2). The initial thickness for the post-reflected shock fit is taken from the incident shock fitted result, but nearly the same rate would be obtained if the actual measured pre-reflected shock thickness were used.

The present results for the growth rate after the reflected shock are summarized in Fig. 7, a plot of growth rate $(d\delta/dt)_1$ normalized by the velocity jump $[u]_1$ induced by the reflected shock *vs.* the Atwood ratio A_1' after the reflected shock. The measured growth rates fall in a band 1.5 to 23% below the analytical formula of Mikaelian (1989), Eq. (2), substantially better agreement than in previous investigations. The agreement improves as M_s increases. Also plotted in the figure are results of Brouillette and Sturtevant (1993); only their low Mach number case (M_s = 1.12), for which boundary-layer effects were relatively small, is in reasonable agreement with the Mikaelian formula. An ambiguity in their data reduction may have led to the choice of much lower growth rates for the higher Mach numbers.

The results of the study of the influence on mixing of membrane placement relative to the mesh is presented in Fig. 8. The curves show a dramatic increase of the growth rate after the incident shock up to a factor of six, depending of whether the membrane was placed on the downstream side ((v-h)-m), between the vertical and horizontal partial meshes (v-m-h) or on the upstream side (m-(v-h)) of the mesh. But the growth rates after the reflected shock were almost the same in all three cases, although, for the last case, the interface was already very thick before the interaction with the reflected shock. It cannot be excluded that for the experiments with the membrane on the upstream side of the wire mesh (m-(v-h)) the membrane was bulged somewhat to the upstream side prior to the arrival of the incident shock (cf. Fig. 4b).

5 Discussion and conclusions

Results of growth rate measurements of impulsively accelerated plane interfaces between air and SF_6 have been presented. Due to the much larger test section than in previous

studies, the effects of shock-wave/boundary-layer interaction have been reduced significantly. The resulting increased resolution of schlieren pictures and comparison of pictures taken at the same instant both with horizontal and vertical knife edges permit a better interpretation of the visible flow features. Contrary to previous investigations in smaller facilities, no strong wall vortex was found in these experiments, which is also an indication for the reduced influence of the boundary-layer.

Strong damping of mixing after the incident shock by the nitrocellulose membrane has been demonstrated by experiments in which the membrane was fragmented immediately after the shock passage by pushing it through a wire mesh. The measured growth rates were found to be six times greater in this case than when the mesh was upstream of the membrane. In both cases, the measured growth rate after the incident shock is less than predicted by Mikaelian (1989), Eq. (2).

On the other hand, the growth rate after the reflected shock agrees to within 1.5–23%, depending on the shock strength, with Eq. (2). The fact that the normalization suggested by Eq. (2) does not remove all of the shock-strength dependence is taken to mean that the growth rate constant $K = 0.28$ in Eq. (2) depends weakly on initial conditions. Pre-reflected shock conditions are not only shock-strength dependent but also apparatus (mesh and membrane) and facility dependent. Dependence on mesh and membrane configuration will be investigated further in the present facility. Since Eq. (2) was derived by extrapolating constant-acceleration Rayleigh-Taylor rocket experiments (Read 1984) and is here applied to shock tube experiments, it is clear that K is very robust to facility change. Whether it is similarly robust for different shock tubes or methods of generating shock waves can only be tested in other large-scale facilities.

Acknowledgement. This research was supported by the U.S. Department of Energy, Lawrence Livermore National Laboratory, under contract agreement DOE W-7405-ENG-48. The first author was also supported in part by the Deutsche Forschungsgemeinschaft, Germany.

References

1. Andronov VA, Bakhrakh SM, Meshkov EE, Mokhov VN, Nikiforov VN, Pevnitskii AV, Tolshmyakhov AI (1976) Turbulent mixing at contact surface accelerated by shock waves. Sov. Phys. JETP 44:424
2. Andronov VA, Bakhrakh SM, Meshkov EE, Nikiforov VV, Pevnitskii AV, Tolshmyakhov AI (1982) An experimental investigation and numerical modeling of turbulent mixing in one-dimensional flows. Sov. Phys. Dokl. 27:393
3. Benjamin RF (1982) Experimental observations of shock stability and shock-induced turbulence. In: Dannevik WP, Buckingham AC, Leith CE (eds) Advances in compressible turbulent mixing. Lawrence Livermore National Laboratory, CONF-8810234
4. Brouillette M and Sturtevant B (1989) Growth induced by multiple shock waves normally incident on plane gaseous interfaces. Physica D 37:248
5. Brouillette M and Sturtevant B (1993) Experiments on the Richtmyer-Meshkov instability: Small-scale perturbations on a plane interface. Phys. Fluids A 5:916
6. Budzinsky JB (1992) Planar Rayleigh scattering measurements of shock enhanced mixing. Ph.D. thesis, California Institute of Technology
7. Liepmann HW, Roshko A, Coles D, Sturtevant B (1962) A 17-inch diameter shock tube for studies in rarefied gas dynamics. Rev. Sci. Instrum. 33:625
8. Landeg D, Philpot M, Smith I, Smith A (1993) The laser sheet as a quantitative diagnostic in shock tube experiments. In: Linden PF, Youngs DL, Dalziel SB (eds) Proc.4th Int.Workshop on the Physics of Compressible Turbulent Mixing, Cambridge University Press, London
9. Meshkov EE (1969) Instability of the interface of two gases accelerated by a shock wave. Sov. Fluid Dyn. 4:101
10. Mikaelian KO (1989) Turbulent mixing generated by Rayleigh-Taylor and Richtmyer-Meshkov instabilities. Physica D 36:343
11. Read KI (1984) Experimental investigation of turbulent mixing in Rayleigh-Taylor instability. Physica D 12:45
12. Richtmyer RD (1960) Taylor instability in shock acceleration of compressible fluids. Commun. Pure Appl. Math. 13:297
13. Youngs DL (1989) Modelling turbulent mixing by Rayleigh-Taylor instability. Physica D 37:270

This article was processed by the author using the LaTeX style file *pljour2* from Springer-Verlag.